Gas-Kinetic Scheme for Continuum and Near-Continuum Hypersonic Flows

Wei Liao* and Li-Shi Luo†
Old Dominion University, Norfolk, Virginia 23529
and
Kun Xu‡
*Hong Kong University of Science and Technology,
Clear Water Bay, Kowloon, Hong Kong, People's Republic of China*

We present a unified approach for both continuum and near-continuum flows based on the Boltzmann equation and kinetic theory. We use the gas-kinetic scheme developed from the linearized Boltzmann equation for the continuum flows and a modified gas-kinetic scheme with a variable relaxation time for the near-continuum flows. The gas-kinetic schemes are validated with simulations of the hypersonic flow past a hollow flare at Mach number 9.91 and the shock structures of argon gas at Mach numbers 8.0 and 9.0. Our results show that the gas-kinetic schemes can indeed simulate both the continuum and near-continuum flows.

I. Introduction

WITH severe rarefaction effects and/or within shocks of a few mean free path thickness, modeling and simulation of complex hypersonic flows become very challenging for computational fluid dynamics (CFD) [1]. Such problems are genuinely multiscale in nature. Outside of shocks, the flows are nearly at thermodynamical equilibrium and thus they can be adequately described by the continuum theory—the Navier–Stokes equations, which are the governing equations of hydrodynamics. However, within shocks, the flow is far from the thermodynamical equilibrium and cannot be well described by the continuum theory. In dealing with nonequilibrium flows, one has to solve the Boltzmann equation and one of the most commonly used approaches is the direct simulation Monte Carlo (DSMC) method [2]. The DSMC is a stochastic method which is very effective for free-molecular flows with large Knudsen numbers. However, the DSMC method has several limitations. First, it is subject to numerical fluctuations due to its stochastic nature. Thus DSMC simulations require averaging to obtain flowfields of interest, and for time-dependent flows, DSMC simulations require ensemble averaging, which can be prohibitively expensive in terms of computational time for realistic flows. And second, the DSMC method becomes ineffective in the near-continuum flow region, because its time step must be smaller than the mean free time, which is extremely small in the near-continuum flow region [3–6]. Therefore, in the near-continuum flow regime in which the Knudsen number is small or moderate, the computational time required by the DSMC simulations is several orders of magnitude longer than that required by conventional CFD methods. Because of these limitations, it is difficult to couple the DSMC method with conventional CFD methods based on direct discretizations of the Navier–Stokes equations, which are deterministic methods characterized by their spatial-temporal accuracies.

In this work we intend to address the difficulty encountered in coupling between the continuum and near-continuum flows. We present a unified approach for both the continuum and near-continuum flows based on the gas-kinetic scheme (GKS) [7–10], which is based on the Boltzmann equation and kinetic theory, as opposed to other CFD methods based on the continuum theory. In the gas-kinetic scheme, the fluxes are reconstructed from the single particle distribution function f in phase space, which is the (approximated) solution of the Boltzmann equation. The fluxes so obtained possess the nonequilibrium information beyond the linear constitutive laws and therefore can capture nonequilibrium effects.

In what follows, we will first show the basic theory behind the GKS and describe the formulation of the GKS. We will use the GKS method to simulate 1) the hypersonic flow around a hollow flare at Mach number 9.91 [1,11] and 2) the shock structure of argon gas at Mach numbers 8.0 and 9.0 [12,13]. The former is a continuum flow with a shock-boundary layer and shock–shock interactions and the latter is near-continuum flow within a hypersonic shock. Our results show that the gas-kinetic scheme has the capability to simulate both continuum and near-continuum flows effectively and efficiently.

II. Numerical Methods

A. Gas-Kinetic Scheme for Compressible Flows

We shall describe the construction of the GKS for compressible flows [7,8]. We begin with the linearized Boltzmann equation [14],

$$\partial_t f + \boldsymbol{\xi} \cdot \nabla f = \mathcal{L}(f, f) \tag{1}$$

where $f := f(\boldsymbol{x}, \boldsymbol{\xi}, \boldsymbol{\zeta}, t)$ is the single particle distribution function of space $\boldsymbol{x}$, particle velocity $\boldsymbol{\xi}$, particle internal degree of freedom $\boldsymbol{\zeta}$ of dimension Z, and time t; $\mathcal{L}$ is the linearized collision operator. For the sake of simplicity, and without losing generality in the context of the linearized Boltzmann equation, we will use the Bhatnagar–Gross–Krook (BGK) single relaxation time model for $\mathcal{L}$ [15],

$$\partial_t f + \boldsymbol{\xi} \cdot \nabla f = -\frac{1}{\tau}[f - f^{(0)}] \tag{2}$$

Here τ is the collision time and $f^{(0)}$ is the Maxwellian equilibrium distribution function in D dimensions,

$$f^{(0)} = \rho(\beta/2\pi)^{(D+Z)/2} e^{-\frac{1}{2}\beta(\boldsymbol{c}\cdot\boldsymbol{c} + \boldsymbol{\zeta}\cdot\boldsymbol{\zeta})} \tag{3}$$

where $\boldsymbol{c} := (\boldsymbol{\xi} - \boldsymbol{u})$ is the peculiar velocity, $\beta = (RT)^{-1}$, R is the gas constant, and ρ, $\boldsymbol{u}$, and T are the density, flow velocity, and temperature, respectively. The conserved variables are the conserved moments of the collision operator

*Research Assistant Professor, Department of Mathematics and Statistics. Member AIAA.
†Associate Professor, Department of Mathematics and Statistics.
‡Professor, Department of Mathematics. Member AIAA.

$$\rho = \int f \, d\Xi = \int f^{(0)} \, d\Xi \qquad (4a)$$

$$\rho \boldsymbol{u} = \int f \boldsymbol{\xi} \, d\Xi = \int f^{(0)} \boldsymbol{\xi} \, d\Xi \qquad (4b)$$

$$\rho E = \rho \epsilon + \frac{1}{2} \rho u^2 = \frac{1}{2} \int f(\xi^2 + \zeta^2) \, d\Xi = \frac{1}{2} \int f^{(0)}(\xi^2 + \zeta^2) \, d\Xi \qquad (4c)$$

where E is the specific total energy and $\epsilon := \frac{1}{2}(D + Z)k_B T$ is the specific internal energy, k_B is the Boltzmann constant, and $\Xi := (\boldsymbol{\xi}, \boldsymbol{\zeta})$ denotes the single particle velocity space and the internal degrees of freedom. The Maxwellian equilibrium leads to the equipartition of energy among the degrees of freedom, that is, each degree of freedom shares the same amount of energy $k_B T/2$ at equilibrium.

By integrating along the characteristics, one can obtain the following solution of the BGK equation (2):

$$f(\boldsymbol{x} + \boldsymbol{\xi}t, t) = e^{-t/\tau} f_0 + \frac{1}{\tau} \int_0^t f^{(0)}(\boldsymbol{x'}, \boldsymbol{\xi}, \boldsymbol{\zeta}, t') e^{(t'-t)/\tau} \, dt' \qquad (5)$$

where $\boldsymbol{x'} := \boldsymbol{x} + \boldsymbol{\xi}t'$, and the initial state $f_0 := f(\boldsymbol{x}, \boldsymbol{\xi}, \boldsymbol{\zeta}, t = 0)$. The GKS is formulated based on the above equation. With f_0 and $f_0^{(0)} := f^{(0)}(\boldsymbol{x}, \boldsymbol{\xi}, \boldsymbol{\zeta})$ given, one can construct an approximate solution for f at a later time $t > 0$.

The gas-kinetic scheme is a finite-volume method for compressible flows. Thus, the values of the hydrodynamic variables, represented by $\mathbf{W}$, are given at cell centers, while the values of fluxes, represented by $\mathbf{F}_\alpha$, are needed at cell boundaries. Unlike conventional CFD methods which evaluate fluxes from the hydrodynamic variables, the gas-kinetic scheme computes the numerical fluxes from the distribution function f. We shall limit our discussion to two dimensions, with the total number of internal degrees of freedom $Z = 1 + (5 - 3\gamma)/(\gamma - 1)$ accounting for the random motion in the z direction and 2 rotational degrees of freedom, and $\gamma = c_p/c_v$ is the ratio of specific heats.

For the sake of convenience, we shall use the following notation for the vectors of $(D + 2)$ dimensions:

$$\boldsymbol{\Psi} := (1, \boldsymbol{\xi}, (\xi^2 + \zeta^2)/2)^\mathsf{T} \qquad (6a)$$

$$\mathbf{W} := (\rho, \rho \boldsymbol{u}, \rho E)^\mathsf{T} = \int f \boldsymbol{\Psi} \, d\Xi = \int f^{(0)} \boldsymbol{\Psi} \, d\Xi \qquad (6b)$$

$$\mathbf{F}_\alpha := \int f \boldsymbol{\Psi} \xi_\alpha \, d\Xi, \qquad \alpha \in \{x, y, z\} := \{1, 2, 3\} \qquad (6c)$$

$$\mathbf{h} := (\rho, \boldsymbol{u}, T)^\mathsf{T} \qquad (6d)$$

$$\mathbf{h'} := (\rho^{-1}, \beta \boldsymbol{u}, \tfrac{1}{2}[\beta(c^2 + \zeta^2) - (D + Z)]T^{-1})^\mathsf{T} \qquad (6e)$$

where T denotes the transpose operator. In the above notation, $\boldsymbol{\Psi}$, $\mathbf{W}$, $\mathbf{F}_\alpha$, and $\mathbf{h}$ have the collisional invariants, the conserved quantities, the fluxes along the α axis, and the primitive variables as their components, respectively.

To simplify the ensuing discussion, we will only show the construction of the GKS in one dimension. Bear in mind that the GKS is a genuine multidimensional scheme. Because the advection operator in the Boltzmann equation is linear, an operator splitting among D coordinates can be easily implemented. We denote a cell center at x coordinate by x_i, and its left and right cell boundaries by

$x_{i-1/2}$ and $x_{i+1/2}$, respectively. For simplicity we set the initial time $t_0 = 0$, and then the solution (5) at position x and time t is

$$f(x, t) = e^{-t/\tau} f_0(x - \xi_1 t) + \frac{1}{\tau} \int_0^t f^{(0)}(x', t') e^{-(t-t')/\tau} \, dt' \qquad (7)$$

where $x' := x - \xi_1(t - t')$ is the x coordinate of the particle trajectory. In the previous equation we omitted the variables in f which remain unchanged in time. Initially, only the values of the hydrodynamic variables, ρ, $\rho \boldsymbol{u}$, and ρE are given at the cell center x_i, but the fluxes are to be evaluated at the cell boundaries $x_{i\pm 1/2}$. Therefore, both f_0 and $f^{(0)}(x', t')$ in the above equation are to be constructed from the hydrodynamic variables through the Boltzmann equation and Taylor expansions of f.

We can formally write the BGK equation (2) as

$$f = f^{(0)} - \tau d_t f, \qquad d_t := \partial_t + \boldsymbol{\xi} \cdot \nabla \qquad (8)$$

Thus, f can be solved iteratively, starting with $f = f^{(0)}$ on the right-hand side of the previous equation. For the purpose of simulating the Navier–Stokes equation, $f = f^{(0)} - \tau d_t f^{(0)}$ is sufficient. The initial value can be approximated as

$$f_0 \approx [1 - \tau(\partial_t + \xi_1 \partial_x)] f^{(0)} = [1 - \tau \mathbf{h'} \cdot (\partial_t + \xi_1 \partial_x) \mathbf{h}] f^{(0)} \qquad (9)$$

In addition, the equilibrium can be expanded in a Taylor series about $x = 0$,

$$f^{(0)}(x, t) \approx [1 + x \partial_x] f^{(0)}(0, t) = [1 + x \mathbf{h'} \cdot \partial_x \mathbf{h}] f^{(0)}(0, t) \qquad (10)$$

By substituting Eq. (10) into Eq. (9) we have

$$f_0(x, t) \approx [1 + x \mathbf{h'} \cdot \partial_x \mathbf{h}][1 - \tau \mathbf{h'} \cdot (\partial_t + \xi_1 \partial_x) \mathbf{h}] f^{(0)}(0, t)$$
$$= [1 + ax - \tau(a\xi_1 + A)] f^{(0)}(0, t) \qquad (11)$$

where $a = \mathbf{h'} \cdot \partial_x \mathbf{h}$ and $A = \mathbf{h'} \cdot \partial_t \mathbf{h}$ are functions of $\boldsymbol{\xi}$ and the hydrodynamic variables, ρ, $\boldsymbol{u}$, and T and their first-order derivatives. They are related by the compatibility condition for f

$$\int f^{(n)} \boldsymbol{\Psi} \, d\Xi = 0, \qquad \forall \, n > 0$$

where $f^{(n)}$ is the nth order Chapman–Enskog expansion of f, and $f^{(0)}$ is the Maxwellian of Eq. (10). Therefore, the first-order compatibility condition

$$\int f^{(1)} \, d\Xi = -\tau \int d_t f^{(0)} \, d\Xi = -\tau \int (A + a\xi_1) f^{(0)} \, d\Xi = 0$$

leads to the relation between A and a,

$$\int A f^{(0)} \, d\Xi = -\int a f^{(0)} \xi_1 \, d\Xi \qquad (12)$$

In computing the gradients $\partial_x \mathbf{h}$ for the coefficient a in Eq. (11), we must assume that the hydrodynamic variables can be discontinuous at the cell boundary $x_{i+1/2}$ in general.

As for $f^{(0)}(x, t)$ in the integrand of Eq. (7), it can be evaluated by its Taylor expansion,

$$f^{(0)}(x, t) \approx (1 + t\partial_t + x\partial_x) f^{(0)}(0, 0)$$
$$= f^{(0)}(0, 0)[1 + \mathbf{h'} \cdot (t\partial_t + x\partial_x)\mathbf{h}] = (1 + \bar{a}x + \bar{A}t) f^{(0)}(0, 0) \qquad (13)$$

where $\bar{a}$ and $\bar{A}$ are similar to a and A, respectively. The difference is that in $\bar{a}$ the hydrodynamic variables are assumed to be continuous but not their gradients, while in a the hydrodynamic variables are assumed to be discontinuous. The details of how to evaluate a, A, $\bar{a}$, and $\bar{A}$ will be discussed next.

Assuming the hydrodynamic variables are discontinuous at the cell boundaries (or interfaces) of $x_{i+1/2} = 0$, then the values of the equilibrium $f^{(0)}$ on both sides of the cell boundary have to be

evaluated differently. For the value $f_L^{(0)}$ on the left side, the hydrodynamic variables **h** are interpolated to the left cell boundary $x_{i+1/2}^-$ with two points left and one point right of $x_{i+1/2}$, that is, x_{i-1}, x_i, and x_{i+1}. Then the left equilibrium value $f_L^{(0)}$ is computed from the hydrodynamic variables at $x_{i+1/2}^-$. Similarly, the right equilibrium value $f_R^{(0)}$ is evaluated from the hydrodynamic variables interpolated to $x_{i+1/2}^+$ with two points right and one point left of $x_{i+1/2}$, that is, x_i, x_{i+1}, and x_{i+2}. The van Leer limiter is used in the interpolations [8,16]. Specifically, the gradients of the hydrodynamic variables are computed as the following:

$$\partial_x \mathbf{h}_L(x_{i+1/2}^-) = \frac{\mathbf{h}(x_{i+1/2}^-) - \mathbf{h}(x_i)}{x_{i+1/2} - x_i}$$

Then the coefficient a_L at the left cell boundary $x_{i+1/2}^-$ is given by

$$a_L(x_{i+1/2}^-) = \mathbf{h}_L'(x_{i+1/2}^-) \cdot \partial_x \mathbf{h}_L(x_{i+1/2}^-)$$

As for the coefficient a_R at the right cell boundary $x_{i+1/2}^+$, the hydrodynamic variables are interpolated from the following three points: x_i, x_{i+1}, and x_{i+2}, and then

$$\partial_x \mathbf{h}_R(x_{i+1/2}^+) = \frac{\mathbf{h}(x_{i+1/2}^+) - \mathbf{h}(x_{i+1})}{x_{i+1/2} - x_{i+1}},$$

$$a_R(x_{i+1/2}^+) = \mathbf{h}_R'(x_{i+1/2}^+) \cdot \partial_x \mathbf{h}_R(x_{i+1/2}^+)$$

With a_L and a_R given, A_L and A_R can be obtained immediately by using the compatibility condition (12).

The equilibria at both sides of the cell boundary $x_{i+1/2}$ are $f_L^{(0)} := f^{(0)}(\boldsymbol{\xi}, \mathbf{h}_L)$ and $f_R^{(0)} := f^{(0)}(\boldsymbol{\xi}, \mathbf{h}_R)$, which are available now because $\mathbf{h}_L$ and $\mathbf{h}_R$ are given. In equilibrium $f^{(0)}$, the hydrodynamic variables are assumed to be continuous. Therefore, the conservative variables **W** at the cell boundary $x_{i+1/2}$ are obtained by integrating the equilibrium at both sides of the cell boundary:

$$\mathbf{W}(x_{i+1/2}) = \int_{\xi_x \geq 0} d\boldsymbol{\Xi}\, \boldsymbol{\Psi} f_L^{(0)} + \int_{\xi_x \leq 0} d\boldsymbol{\Xi}\, \boldsymbol{\Psi} f_R^{(0)} \qquad (14)$$

where the hydrodynamic variables $\mathbf{h} := (\rho, \boldsymbol{u}, T)^\mathsf{T}$ can be easily obtained from the conservative variables $\mathbf{W} := (\rho, \rho\boldsymbol{u}, \rho E)^\mathsf{T}$, and then the coefficients $\bar{a}_L$ and $\bar{a}_R$ are computed as follows:

$$\bar{a}_L(x_{i+1/2}) = \mathbf{h}'(x_{i+1/2}) \cdot \frac{\mathbf{h}(x_{i+1/2}) - \mathbf{h}(x_i)}{x_{i+1/2} - x_i},$$

$$\bar{a}_R(x_{i+1/2}) = \mathbf{h}'(x_{i+1/2}) \cdot \frac{\mathbf{h}(x_{i+1/2}) - \mathbf{h}(x_{i+1})}{x_{i+1/2} - x_{i+1}}$$

Consequently, we have

$$f_0(x,t) = [1 + a_R(x - \tau\xi_1) - \tau A_R]H(x)f_R^{(0)}(0,t)$$
$$+ [1 + a_L(x - \tau\xi_1) - \tau A_L]H(-x)f_L^{(0)}(0,t) \qquad (15a)$$

$$f^{(0)}(x,t) = [1 + H(-x)\bar{a}_L x + H(x)\bar{a}_R x + \bar{A}t]f^{(0)}(0,0) \qquad (15b)$$

where $H(x)$ is the Heaviside function. Finally, the value of f at a cell boundary can be obtained by substituting the previous equations of $f_0(x,t)$ and $f^{(0)}(x,t)$ into Eq. (7),

$$f(x_{i+1/2}, t) = \{[(1 - \bar{A}\tau)(1 - e^{-t/\tau}) + \bar{A}t]$$
$$+ [(t+\tau)e^{-t/\tau} - \tau][\bar{a}_L H(\xi_1) + \bar{a}_R H(-\xi_1)]\xi_1\}f_0^{(0)}$$
$$+ e^{-t/\tau}\{[(1 - \xi_1(t+\tau)a_L) - \tau A_L]H(\xi_1)f_{0L}^{(0)}$$
$$+ [(1 - \xi_1(t+\tau)a_R) - \tau A_R]H(-\xi_1)f_{0R}^{(0)}\} \qquad (16)$$

where $f_0^{(0)}$, $f_{0L}^{(0)}$, and $f_{0R}^{(0)}$ are initial values of $f^{(0)}$, $f_L^{(0)}$, and $f_R^{(0)}$ evaluated at the cell boundary $x_{i+1/2}$. The only unknown in $f(x_{i+1/2}, t)$ of Eq. (16) is the coefficient $\bar{A}$. By using $f^{(0)}(x_{i+1/2}, t)$ of Eq. (15b) and $f(x_{i+1/2}, t)$ of Eq. (16), the conservation laws lead to the following equation:

$$\int_0^{\Delta t} dt \int d\boldsymbol{\Xi}\, \boldsymbol{\Psi} f^{(0)}(x_{i+1/2}, t) = \int_0^{\Delta t} dt \int d\boldsymbol{\Xi}\, \boldsymbol{\Psi} f(x_{i+1/2}, t)$$

which is used to determine $\bar{A}$ in terms of a_L, a_R, $\bar{a}_L$, and $\bar{a}_R$. Therefore, $f^{(0)}(x_{i+1/2}, t)$ is fully determined from the hydrodynamic variables at the cell centers about the cell boundary $x_{i+1/2}$.

The relaxation time τ in Eq. (16) has yet to be determined. In the gas-kinetic scheme for compressible flows, the particle collision time is determined by the local macroscopic flow variables through

$$\tau = \mu/p \qquad (17)$$

where μ is the dynamic viscosity and p is the pressure. The above relation between τ, μ, and p is valid when the flowfields are continuous. When discontinuity is considered as for compressible flows with shocks, one must introduce some artificial dissipation to capture shocks [8]. In the GKS method, the artificial dissipation is introduced by modifying the relaxation time τ as the following:

$$\tau = \frac{\mu(x_{i+1/2})}{p(x_{i+1/2})} + \sigma\Delta t \frac{(p_L - p_R)}{(p_L + p_R)} = \tau_0 + \sigma\tau_1 \qquad (18)$$

where τ_0 and $\sigma\tau_1$ represent the physical and artificial mean free times, respectively. The value of the dynamic viscosity $\mu(x_{i+1/2})$ is determined by Sutherland's formula:

$$\mu = \mu_0 \frac{(T_0 + C)}{(T + C)}\left(\frac{T}{T_0}\right)^{3/2} = \mu_0 \frac{(1 + CR\beta_0)}{(1 + CR\beta)}\left(\frac{\beta_0}{\beta}\right)^{1/2}$$

where μ_0, T_0, and C are material-dependent constants, and $\beta := 1/RT$ and $\beta_0 := 1/RT_0$. Specifically, we use $\tau_0 = \mu/p = \mu\beta/\rho$, in which the value of $\tau_0(x_{i+1/2})$ is computed from the values of $T(x_{i+1/2})$ and $\rho(x_{i+1/2})$ at the previous time step $t = t_{n-1}$, given by the hydrodynamic variables $\mathbf{h}(x_{i+1/2})$ through $\mathbf{W}(x_{i+1/2})$ of Eq. (14).

The term of $\sigma\tau_1$ in Eq. (18) gives rise to an artificial dissipation, which can be tuned by the parameter $\sigma \in [0, 1]$. The values of pressure evaluated at the left and the right of the cell boundary $x_{i+1/2}$, p_L, and p_R are obtained from $\mathbf{h}(x_{i+1/2}^-)$ and $\mathbf{h}(x_{i+1/2}^+)$, respectively. Therefore, the artificial dissipation is in effect only when shocks are treated as discontinuities. Obviously, when flowfields are continuous, $p_L = p_R$, and the artificial dissipation vanishes.

With f given at the cell boundaries, the time-dependent fluxes can be evaluated,

$$\mathbf{F}_\alpha^{i+1/2,j} = \int \xi_\alpha \boldsymbol{\Psi} f(x_{i+1/2}, t)\, d\boldsymbol{\Xi} \qquad (19)$$

By integrating the above equation over each time step, we obtain the total fluxes as

$$\bar{\mathbf{F}}_x^{i\pm1/2,j} = \int_0^{\Delta t} \mathbf{F}_x^{i\pm1/2,j}\, dt, \qquad \bar{\mathbf{F}}_y^{i,j\pm1/2} = \int_0^{\Delta t} \mathbf{F}_y^{i,j\pm1/2}\, dt \qquad (20)$$

Then the flow governing equations in the finite-volume formulation can be written as

$$\mathbf{W}_{ij}^{n+1} = \mathbf{W}_{ij}^n - \frac{1}{\Delta x}(\bar{\mathbf{F}}_x^{i+1/2,j} - \bar{\mathbf{F}}_x^{i-1/2,j}) - \frac{1}{\Delta y}(\bar{\mathbf{F}}_y^{i,j+1/2} - \bar{\mathbf{F}}_y^{i,j-1/2})$$
$$(21)$$

which are used to update the flowfield.

B. Modified Gas-Kinetic Scheme for Near-Continuum Flows

In the near-continuum or transition flow regimes, the mean free time τ is no longer a function of hydrodynamic variables alone as indicated by Eq. (17). For example, within a hypersonic shock, the mean free time would depend on the hydrodynamic variables as well as their derivatives. In other words, the simple constitutive relations in the framework of continuum theory are no longer valid in the

nonequilibrium flows. This is clear from the derivation of the BGK equation [14]:

$$\int d\boldsymbol{\xi}_2 \, d\theta \, d\epsilon B(\theta, \|\boldsymbol{\xi}_1 - \boldsymbol{\xi}_2\|) f_1' f_2'$$

$$\approx f_1^{(0)} \int d\boldsymbol{\xi}_2 \, d\theta \, d\epsilon B(\theta, \|\boldsymbol{\xi}_1 - \boldsymbol{\xi}_2\|) f_2^{(0)} = \frac{1}{\tau(\boldsymbol{\xi}_1)} f_1^{(0)} \quad (22)$$

where the postcollision distribution function f_i' is approximated by the equilibrium $f_i^{(0)}$, and the relaxation time τ is a function of $\boldsymbol{\xi}_1$ unless $B(\theta, \|\boldsymbol{\xi}_1 - \boldsymbol{\xi}_2\|)$ is independent of $\|\boldsymbol{\xi}_1 - \boldsymbol{\xi}_2\|$, which is only true for the Maxwell molecules. It is clear that in general the mean free time τ depends on the molecular velocity $\boldsymbol{\xi}_1$ and the intermolecular interaction included in $B(\theta, \|\boldsymbol{\xi}_1 - \boldsymbol{\xi}_2\|)$. Therefore, to accurately compute shock structures, in which the flow is far from equilibrium and the Navier–Stokes equation is no longer valid, one would need to solve the Boltzmann equation, by using the DSMC method, for instance. In the present work we shall use a modified GKS for this purpose [17,18].

The basic idea behind the modified GKS for shock structures is the following. We know that the conservation laws are valid everywhere, even within shock and at a microscopic level. What breaks down within shocks are the linear constitutive relations. The shock structures are of the order of the mean free path. Within shocks the mean free time τ would not be a constant and would strongly depend on local flowfields and their gradients as well as the microscopic intermolecular potential, as indicated by Eq. (22). We use a self-consistent iterative solution of the Boltzmann equation to approximate τ. In what follows we shall consider a one-dimensional shock structure for the sake of simplicity.

We will use the BGK equation to illustrate our idea:

$$f = f^{(0)} - \tau d_t f = f^{(0)} - \tau(\partial_t + \xi_1 \partial_x) f \quad (23)$$

Suppose we can modify the relaxation time such that it depends on flowfields and their gradients, and the form of the Navier–Stokes equations remains intact, that is,

$$f \approx f^{(0)} - \tau^* d_t f^{(0)} := f^{[1]} \quad (24)$$

where τ^* is the modified relaxation time. On the other hand, one can iterate Eq. (23) once more:

$$f \approx f^{(0)} - \tau d_t f^{(1)} = f^{(0)} - \tau d_t f^{(0)} + \tau \tau^* d_t^2 f^{(0)} := f^{[2]} \quad (25)$$

and assume that the modeling of τ^* is sufficiently accurate to take into account the effects due to higher order derivatives of hydrodynamic variables. Therefore, we have $f^{[1]} \approx f^{[2]}$, which leads to

$$\tau^* d_t f^{(0)} \approx \tau(d_t f^{(0)} - \tau^* d_t^2 f^{(0)}) \quad (26)$$

Then we can obtain the modified relaxation time,

$$\tau^* = \frac{\tau}{1 + \tau(d_t^2 f^{(0)} / d_t f^{(0)})}$$

The above equation depends on the particle velocity $\boldsymbol{\xi}$ and therefore must be averaged over $\boldsymbol{\xi}$. We consider an average over $\phi(\boldsymbol{\xi})$ to obtain

$$\tau^* = \frac{\tau}{1 + \tau \langle d_t^2 f^{(0)} \rangle / \langle d_t f^{(0)} \rangle} \quad (27a)$$

$$\langle d_t f^{(0)} \rangle := \int d_t f^{(0)} \phi(\boldsymbol{\xi}) f \, d\Xi, \qquad \langle d_t^2 f^{(0)} \rangle := \int d_t^2 f^{(0)} \phi(\boldsymbol{\xi}) f \, d\Xi \quad (27b)$$

Because the stress and the heat conduction terms are different moments of the distribution function f, the values of τ^* for these terms should also be treated differently. We use $\phi(\boldsymbol{\xi}) = c^2$ for the relaxation time corresponding to the viscosity coefficient and $\phi(\boldsymbol{\xi}) = c_\alpha(c^2 + \zeta^2)$ for relaxation time corresponding to the heat conductivity coefficient in the α direction. In effect, $\langle d_t^2 f^{(0)} \rangle$ and

$\langle d_t f^{(0)} \rangle$ are computed as the functions of hydrodynamic variables as well as their spatial and temporal derivatives up to second order. We note that the idea of computing τ^* through iteration is in some way similar to that in the regularization of the Chapman–Enskog expansion [19]. We should also emphasize that the linearized Boltzmann equation, of which the BGK model is a special case, is only valid for systems not too far away from equilibrium. For systems far away from equilibrium, more sophisticated collision models must be considered.

To maintain numerical stability, an *empirical* nonlinear dynamic limiter is imposed on τ^*:

$$\tau^* = \frac{\tau}{1 + \max[-0.5, \tau \min(-0.1, \langle d_t^2 f^{(0)} \rangle / \langle d_t f^{(0)} \rangle)]} \quad (28)$$

to guarantee that $\tau^* \geq \tau$ and to minimize the large numerical fluctuation caused by vanishingly small $\langle d_t f^{(0)} \rangle$, which can occur in regions outside of the shock. The idea behind the limiter of Eq. (28) is rather simple and it includes two considerations. The first consideration is based on the general observation that the shock thickness obtained by a Navier–Stokes solver is usually thinner than it should be with a given viscosity, and the shock thickness increases as the viscosity increases. In addition, the stress inside shocks is larger than the value estimated by the linear constitutive laws [20]. Therefore, we require that $\tau^* > \tau$ within shocks. We observe that usually $\langle d_t^2 f^{(0)} \rangle / \langle d_t f^{(0)} \rangle < 0$. Therefore $\tau^* > \tau$ if $0 > \tau \langle d_t^2 f^{(0)} \rangle / \langle d_t f^{(0)} \rangle > -1$. And the second consideration is numerical stability. The numerator in Eq. (27a) may be too close to zero or even become negative, which is unphysical, in the presence of numerical noise. Therefore, we must set a minimum for the numerator, which is 0.5 here. The limiter of Eq. (28) satisfies both criteria. Obviously the τ^* is a continuous function of the local hydrodynamic variables and their derivatives. It does not have the term $\sigma \tau_1$ in Eq. (18) which gives rise to an artificial dissipation, because the flowfields are assumed to be continuous and well resolved within a shock.

C. Prandtl Number Correction

The relaxation time τ in the BGK model determines both the dynamic viscosity μ and the heat conductivity κ, which results in the unit Prandtl number $Pr = \mu/\kappa = 1$. However, this defect can be easily removed by simply replacing the coefficient τ in the heat flux $\boldsymbol{q}$ by the appropriate one determined by the Prandtl number Pr in the total energy flux $\boldsymbol{K}$ [8,21]:

$$\boldsymbol{K}^{\text{new}} = \boldsymbol{K} + \left(\frac{1}{Pr} - 1\right)\boldsymbol{q}, \qquad \boldsymbol{K} := \frac{1}{2} \int (\xi^2 + \zeta^2) \boldsymbol{\xi} f \, d\Xi \quad (29)$$

where $\boldsymbol{q}$ is the time-dependent heat flux:

$$\boldsymbol{q} := \frac{1}{2} \int (c^2 + \zeta^2) \boldsymbol{c} f \, d\Xi \quad (30)$$

Because the distribution function f is assumed to be smooth, it can be approximated by [8]

$$f = f_0^{(0)}[1 - \tau(\bar{a}\xi_1 + \bar{A}) + t\bar{A}] \quad (31)$$

Consequently the heat flux $\boldsymbol{q}$ can be approximated by

$$q_\alpha \approx -\tau \int f_0^{(0)}(\bar{a}\xi_\alpha + \bar{A})(\psi_4 - \boldsymbol{u}_0 \cdot \boldsymbol{\xi})\xi_\alpha \, d\Xi := \tau q_\alpha',$$

$$\psi_4 := \frac{1}{2}(\xi^2 + \zeta^2), \qquad \alpha \in \{x, y\} := \{1, 2\} \quad (32)$$

where $\boldsymbol{u}_0 := (u_0, v_0)$ is the flow velocity at the cell interface and at time $t = 0$. In the above evaluation of q_α, the term $t\bar{A}$ in Eq. (31) has been neglected. This approximation would only affect the temporal accuracy of the GKS. Because all moments needed in Eq. (32) have been computed in the evaluation of the total energy flux $\boldsymbol{K}$, thus additional effort required to compute $\boldsymbol{K}^{\text{new}}$ is negligible. Finally, Eq. (29) can be written as

$$K^{\text{new}} = K + \left(\frac{1}{Pr} - 1\right)\tau q' \qquad (33)$$

For the near-continuum flows, a modified variable relaxation time τ^* given by Eq. (28) must be used. Because different relaxation times must be used for the viscous stress and the heat flux, as indicated in the discussion following Eqs. (27), Eqs. (33) is modified as the following:

$$K^{\text{new}} = K + \left(\frac{\tau_\kappa^*}{Pr} - \tau_\mu^*\right)q' \qquad (34)$$

where τ_κ^* and τ_μ^* are the modified relaxation times corresponding to the heat conductivity κ and the viscosity μ, respectively, and they are computed according to Eq. (27).

III.   Results and Discussions

We developed a GKS code based on kinetic theory which can simulate both continuum and near-continuum compressible flows. To validate our code, we simulate two test cases. The first is a hypersonic flow around an axisymmetrical hollow flare with Mach number $Ma = 9.91$ [1,11] and the second is the shock structure of argon gas with $Ma = 8.0$ and 9.0 [12,13]. The former is a continuum flow with a shock-boundary layer and shock–shock interactions, and the latter is the near-continuum flows within hypersonic shocks.

A.   Hypersonic Flow Around a Hollow Flare

The hypersonic flow around an axisymmetrical hollow flare is a well-known testing case for a shock-boundary layer and shock–shock interactions and has been used to test various numerical methods [1]. Although the Knudsen number Kn is relatively small ($Kn \approx 0.005$) in this case, the existing studies show that the thermodynamic nonequilibrium (rarefaction) gas effects are severe [22]. Complex flow physics in this flow makes it a challenging case for a viscous flow solver to accurately capture the wave interaction.

The freestream parameters are $Ma = 9.91$, $p_\infty = 6.3$ (Pa), $T_\infty = 51$ (K), and $T_w = 293$ (K). These conditions ensure the flow to be a laminar flow in the entire domain. We use $\sigma = 0.1$ in Eq. (18). All boundary conditions are realized through ghost cells. There are two layers of fictitious cells next to boundaries. The fluxes across a boundary are treated in a manner similar to that in the interior domain. The inflow boundary conditions are specified by the freestream parameters and linear extrapolations are used at far-field and outflow boundaries. The wall temperature is fixed at the constant value T_w, and isothermal boundary conditions are used at the wall. We note that GKS simulations of hypersonic flows are sensitive to numerical treatment of boundary conditions, which can severely affect numerical stability of the simulations. With the no-slip boundary conditions at the wall, the velocity in the ghost cells is determined by

$$\boldsymbol{u}_{-1} = -\boldsymbol{u}_1 \qquad (35)$$

where $\boldsymbol{u}_{-1}$ is the velocity at the first layer of ghost cells next to the wall and the wall location is between $\boldsymbol{x}_1$ and $\boldsymbol{x}_{-1}$. Thus Eq. (35) ensures that the velocity vanishes at the wall. The pressure boundary condition is

$$p_{-1} = p_1 \qquad (36)$$

The isothermal boundary conditions are implemented as follow [8]. We consider the quantity $\beta := m/k_B T = 1/RT = \rho/p$. At the isothermal wall, the temperature is $T_0 = T_w$ and $\beta_0 = 1/RT_0$, where the subscript 0 denotes the wall location (and should not be confused with T_0 in Sutherland's formula for the viscosity). The gradient of β normal to the isothermal wall is approximated by

$$\partial_{\boldsymbol{n}}\beta_0 = \frac{\beta_1 - \beta_0}{\|\boldsymbol{x}_1 - \boldsymbol{x}_0\|} \qquad (37)$$

where $\boldsymbol{n}$ denotes the out-normal direction to the wall, and the value of β at the first layer of ghost cells is approximated by

$$\beta_{-1} = \beta_0 - \partial_{\boldsymbol{n}}\beta_0 \|\boldsymbol{x}_0 - \boldsymbol{x}_{-1}\| \qquad (38)$$

With $\boldsymbol{u}_{-1}$, p_{-1}, and β_{-1} given at $\boldsymbol{x}_{-1}$, the values of ρ_{-1} and E_{-1} can be obtained.

Because of strong shock–shock and shock-boundary layer interactions in the flow, we must use some limiter to capture shocks. We use the van Leer limiter in our simulations [8,16]. However, we also observe that the limiter can trigger numerical oscillations near walls which can destabilize the simulation eventually. To circumvent this problem, we use *linear* interpolations without a limiter to compute the hydrodynamic variables at the cell boundaries for the first two layers of cells adjacent to the wall,

$$\mathbf{h}_{i+1/2} = \mathbf{h}_i + (\mathbf{h}_{i+1} - \mathbf{h}_i)\frac{\|\boldsymbol{x}_{i+1/2} - \boldsymbol{x}_i\|}{\|\boldsymbol{x}_{i+1} - \boldsymbol{x}_i\|} \qquad (39)$$

Effectively, the hydrodynamic variables are assumed to be continuous from the wall into two layers of cells adjacent to the wall. These boundary conditions reduce the effect caused by the discontinuities in the initial and boundary conditions, such as $T_\infty \neq T_w$ at the lower left corner of the mesh, where the inflow and the wall boundary conditions meet. With the linear interpolations of Eq. (39), the GKS scheme is essentially reduced to a second-order central difference scheme.

In the present work, the largest mesh used is 241×161, which is highly stretched in the radial (y) direction, as illustrated in Fig. 1a. The normalized temperature T/T_∞ and the normalized pressure p/p_∞ contours obtained by the GKS method are presented in Figs. 1b and 1c, respectively. Complex shock interaction can be observed in the flowfield: An attached shock wave is formed at the leading edge. In the mean time, the flow separates upstream of the flare and reattaches at a point on the conical section, which induces a separation shock wave and an attachment shock wave. These three shock waves interact with each other above the end of the flare. The positions of the separation point and attachment point obtained by the GKS in the present study and the existing data obtained by other methods [11] are presented in Table 1. To ensure grid-size independent results, we provide the GKS results obtained with two meshes, 241×81 and 241×161. When the grid size in the y direction is refined by a factor of 2 with the mesh of 241×81, the changes in the separation and reattachment positions are about 2.9 and 0.5%, respectively, indicating that the results obtained with the mesh 241×161 are nearly grid size independent. Clearly the GKS results are in good agreement with existing data.

In Fig. 2, we compare the pressure coefficient C_p, the skin-friction coefficient C_f, and the Stanton number St obtained from the GKS method with the existing data from the DSMC and other methods [11]:

$$C_p := \frac{(p - p_\infty)}{(1/2)\rho_\infty U_\infty^2}, \qquad C_f := \frac{\tau_w}{(1/2)\rho_\infty U_\infty^2},$$
$$St := \frac{\kappa(\partial_{\boldsymbol{n}}T)_w}{\rho_\infty u_\infty(H_0 - H_w)}$$

where H is the enthalpy, κ is the thermal conductivity, τ_w is the wall shear stress, and $\boldsymbol{n}$ denotes the normal direction of the wall. To amplify the differences, we use a logarithmic scale in the y axis for these figures. For C_f and St, the GKS results are in excellent agreement with the existing data [11,22]. For the wall pressure distribution C_p, we observe a small discrepancy between the GKS result and the experimental data [11] near the entrance. This still remains as an open issue [11] subject to future investigation and it may be due to the uncertainty of the inflow conditions [23].

Figure 3 shows density profiles at two different cross sections $x/L = 0.6$ and 0.76. The inverse phenomenon appears within the region $0.6 < x/L < 0.76$. Again, the GKS results agree well with existing experimental data [11]. It is worth noting that the GKS results accurately predict the radial shock position.
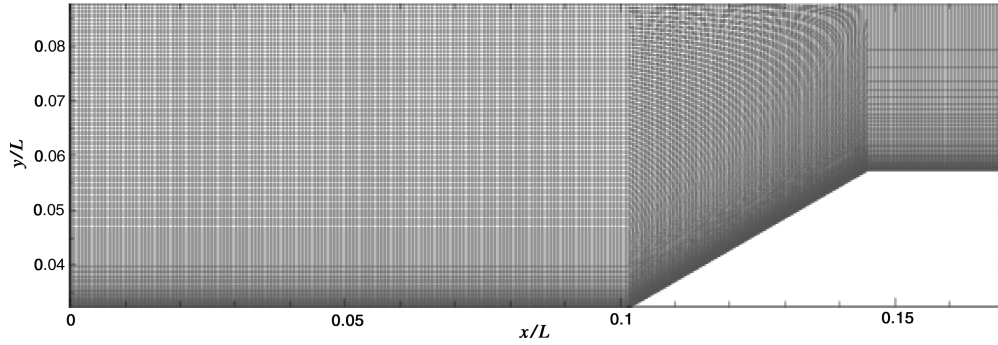
a) The schematic view of the computational mesh
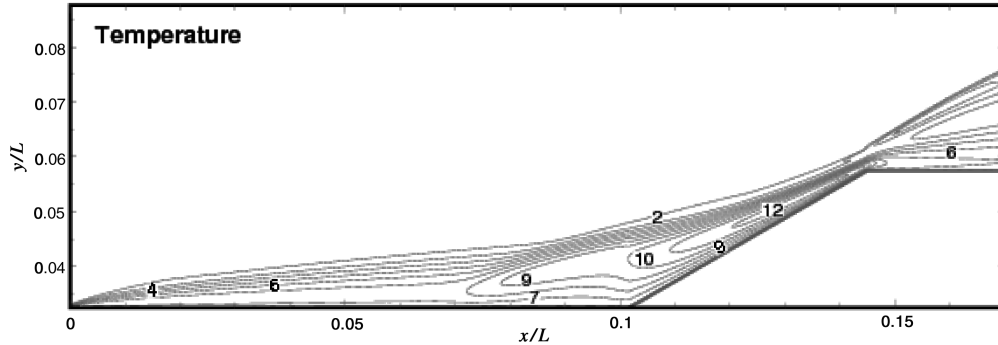
b) The contours of T/T_∞
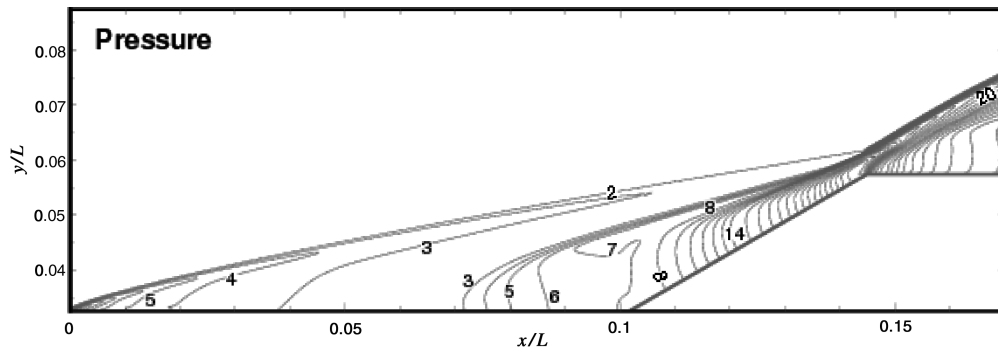
c) The contours of p/p_∞

Fig. 1 Hypersonic flow around a hollow flare with $Ma = 9.91$.

B. Nonequilibrium Shock Structures in Argon Gas with Mach Numbers 8.0 and 9.0

High Mach number shock waves represent flow conditions far from the thermodynamic equilibrium. In this work, a stationary shock wave in atomic argon gas with Mach numbers $Ma = 8.0$ and 9.0 is used to validate the modified GKS method for calculations of the shock structure under hypersonic conditions.

The computational domain is covered with a uniform grid with no less than 30 grid points inside the shock. The entire domain is sufficiently large so that the shock does not disturb the upstream nor the downstream. The upstream flow conditions are as follows: the Mach number $Ma = 8.0$ or 9.0, and the temperature $T_1 = 300$ (K). The downstream flow conditions can be determined by the Rankine–Hugoniot relations. Other parameters are $\gamma = 5/3$, $Pr = 2/3$, and $\mu \propto T^s$, where $s = 1/2 + 2/(v - 1)$ and v is the power of the

intermolecular force law [2]. For the case of $Ma = 8.0$, $v = 12$, and the upstream mean free path λ_1 is defined by [2]

$$\lambda_1 = \frac{2\mu(7 - 2s)(5 - 2s)}{15\rho_1 \sqrt{2\pi R T_1}} \qquad (40)$$

And for the case of $Ma = 9.0$, $v = 7.5$ and λ_1 is defined by [13]

$$\lambda_1 = \frac{16\mu}{5\rho_1 \sqrt{2\pi R T_1}} \qquad (41)$$

These two different definitions of λ_1 are used so that the comparisons with existing data [12,13] can be made.

Figure 4 shows the density and temperature profiles for argon gas computed by the gas-kinetic schemes with and without the modification of the collision time τ, together with the DSMC results

Table 1   Separation and reattachment lengths for the flow past a hollow flare. The GKS results obtained with two meshes, 241 × 81 and 241 × 161, vs the existing data [11]

Abscissa x/L	NS	DSMC	GKS (241 × 81)	GKS (241 × 161)	Exp.
Separation	0.74–0.75	0.76	0.767	0.745	0.76 ± 0.01
Reattachment	1.33	1.32	1.334	1.341	1.34 ± 0.01

a) Pressure coefficient C_p b) Skin friction C_f c) Stanton number St
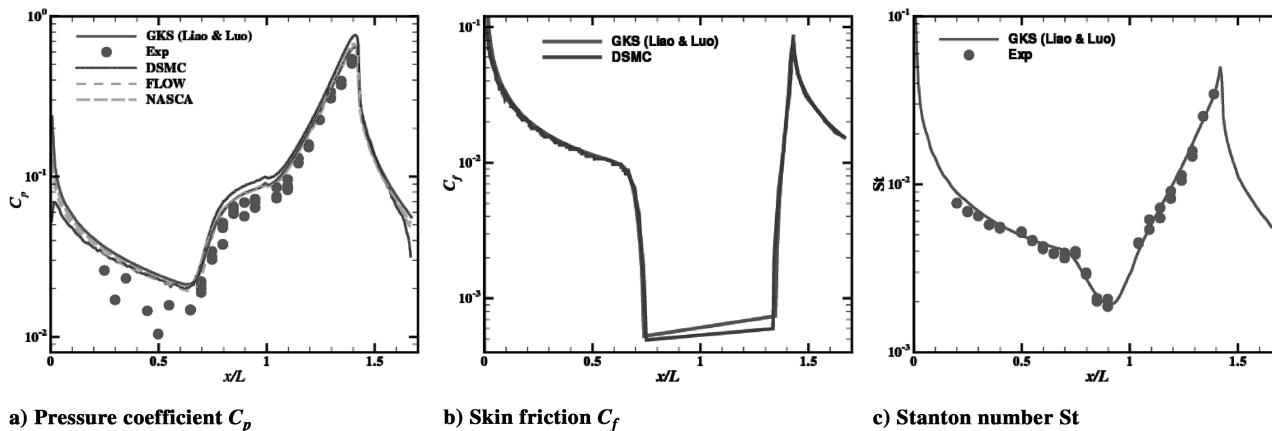
Fig. 2   The hypersonic flow around a hollow flare with $Ma = 9.91$.
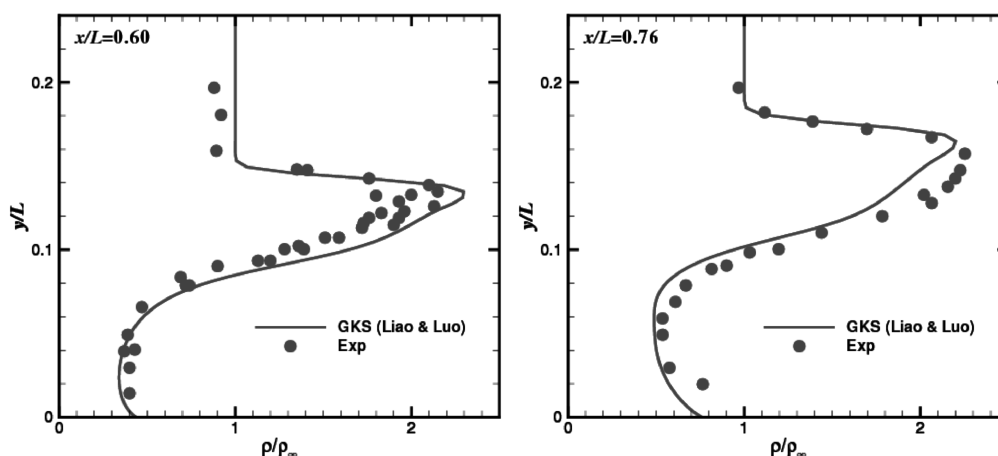
Fig. 3   Density profiles at different positions in the hypersonic flow around a hollow flare with $Ma = 9.91$.
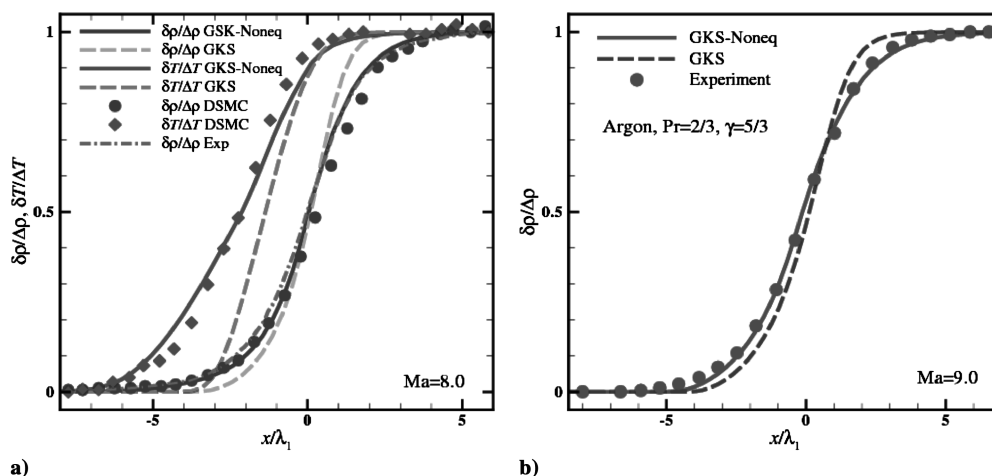
Fig. 4   The density and temperature profiles inside the shock layer of Argon gas at a) $Ma = 8.0$ and b) 9.0.

by Bird [12] and experimental data by Alsmeyer [13]. The distance x is normalized by the upstream mean free path λ_1. The density and temperature distributions are defined as, respectively,

$$\frac{\delta \rho}{\Delta \rho} := \frac{(\rho - \rho_1)}{(\rho_2 - \rho_1)}, \qquad \frac{\delta T}{\Delta T} := \frac{(T - T_1)}{(T_2 - T_1)}$$

where ρ_2 and T_2 are the downstream density and temperature, respectively. Figure 4 shows that at $Ma = 8.0$ and 9.0, the present

results agree very well with the DSMC results and experimental data. For the Mach 8.0 case, the shock thickness and separation distance between the density ρ and the temperature T predicted by the modified GKS method agree very well with those predicted by DSMC [12]. In contrast, the GKS method with a constant $\tau = \mu/p$, which is effectively a Navier–Stokes solver, underpredicts the shock width and the distance between ρ and T.

Figure 5 shows the distributions of normal heat flux q_x and the stress τ_{xx} from the GKS and the modified GKS methods compared

a) Heat flux q_x b) Stress τ_{xx}
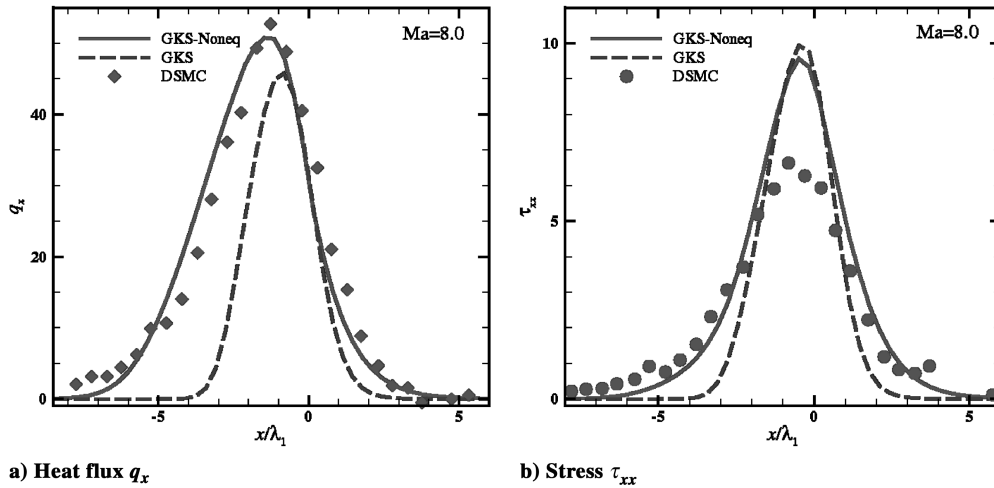
Fig. 5   The heat flux a) and stress b) inside the shock layer of a Mach 8 shock in argon. The "GKS-Noneq" and "GKS" indicate the results obtained by using the GKS with and without variable relaxation time τ^*, respectively. The GKS method with $\tau = \mu/p$ is a finite-volume Navier–Stokes solver.
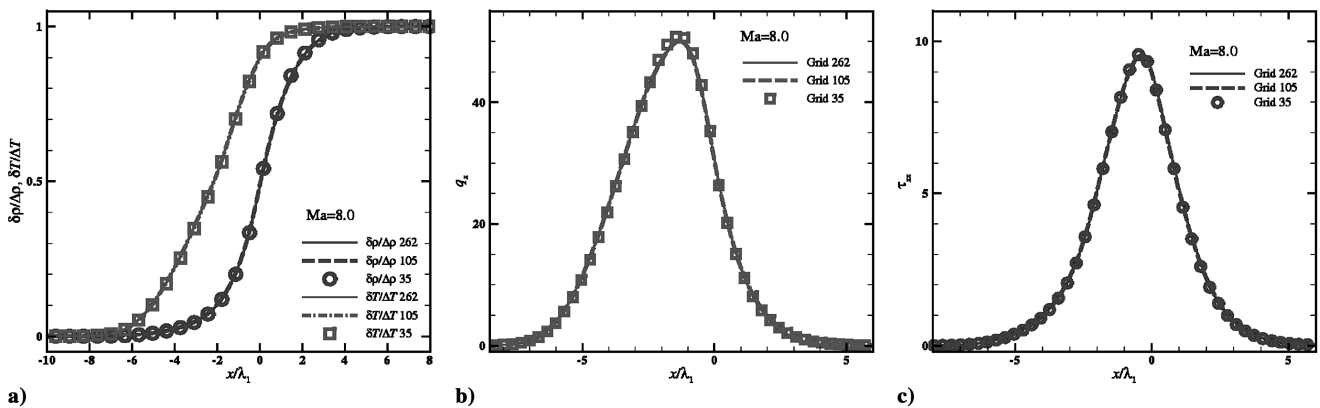

Fig. 6   Grid dependence of the shock structures inside the shock layer in argon at $Ma = 8.0$. a) The density $(\rho(x) - \rho_2)/(\rho_1 - \rho_2)$ and temperature $(T(x) - T_2)/(T_1 - T_2)$ profiles; b) the heat flux q_x; and c) the stress τ_{xx}.

with the DSMC results [12]. The out-normal heat flux q_x and the stress τ_{xx} are defined by

$$q_x := \frac{\kappa \partial_x T}{\rho_1 (2RT_1)^{3/2}}, \qquad \tau_{xx} := \frac{4}{3} \frac{\mu \partial_x u}{(2\rho_1 RT_1)}$$

Figure 5 clearly shows that the modified GKS method with variable relaxation times significantly improves the prediction for the heat flux q_x: Both the magnitude and the width of the distribution of q_x are accurately obtained by the modified GKS method and the GKS results agree very well with the DSMC data [12]. Although significant improvements have also been made in the calculations for the stress τ_{xx} (the width of τ_{xx} is accurately computed), the modified GKS method still overpredicts the magnitude of τ_{xx} by about 40%. This may be due to the fact that the stress is related to the higher order effects while the current τ^* only takes into account up to the second-order ones. The sources of this discrepancy are the subject of our future studies.

Because the modified gas-kinetic scheme involves the derivatives of hydrodynamic variables and a nonlinear dynamic limiter, it would be interesting to investigate its behavior when it is subject to grid refinement. To do so, we compute the shock structures in argon at $Ma = 8.0$ by using about 35, 105, and 262 grids inside the shock layer. The results for the density profile $(\rho(x) - \rho_1)/(\rho_2 - \rho_1)$ and the temperature profile $(T(x) - T_1)/(T_2 - T_1)$, the head flux q_x, and the stress τ_{xx} are showed in Figs. 6a–6c, respectively. Clearly, the results obtained by using these three vastly different mesh sizes do not exhibit any visible difference, except the heat flux q_x. For the heat flux q_x, the peak value of q_x obtained with the coarsest mesh of 35

grid points within the shock differs only by about 1% from that obtained with much finer meshes. Our results show that the modified gas-kinetic scheme is robust when subject to grid refinement.

Our results demonstrate that the modified gas-kinetic scheme with variable mean free time τ^* can effectively and accurately compute the shock structure, which is within the extend of a few mean free paths and cannot be accurately computed by conventional CFD methods based on the solutions of the Navier–Stokes equations, as we have clearly shown in Figs. 4 and 5.

IV.   Conclusions

We have demonstrated in this paper the capability of the gas-kinetic schemes for accurately capturing shock-boundary layer interaction and shock structures. In effect, we present a unified approach for continuum and near-continuum hypersonic flows based on the Boltzmann equation and kinetic theory. The numerical results for the hypersonic flow around a hollow flare with $Ma = 9.91$ and the shock structures of argon gas with $Ma = 8.0$ and 9.0 agree very well with the existing experimental data and other numerical results. We note that conventional CFD methods based on direct discretizations of the Navier–Stokes equations cannot accurately predict shock structures. For nonequilibrium flows such as hypersonic shocks, the advantages of the GKS method over the conventional Navier–Stokes solvers are clearly shown here. Moreover, it takes only under about a minute of CPU time for the shock structure calculation by using the modified GKS method, much faster than the DSMC simulations. We should emphasis that the GKS methods are not intended to replace the DSMC method

where it is effective, that is, in the free molecule region. On the other hand, the GKS methods or other deterministic methods based on CFD can be more effective and efficient in the near-continuum region where the Knudsen number is relatively small and the DSMC simulations can be prohibitively expensive computationally.

As we indicate in the Introduction, our motivation to formulate a unified approach for continuum and near-continuum flows is to circumvent the difficulties encountered in the coupling between the deterministic CFD and the stochastic DSMC methods for nonequilibrium flows. Our preliminary results presented in this work demonstrate the potential of the kinetic methods, such as the GKS methods, to bridge between conventional CFD methods and other methods for nonequilibrium flows based on the Boltzmann equation. Because the modified GKS method is essentially the GKS method for the compressible Navier–Stokes equations with variable relaxation times depending on the flow variables and their derivatives, which are readily available in the GKS method, the GKS methods with and without the variable relaxation times can be run as one code with a switch to turn on and off automatically depending on the local flow information. The modified GKS method can be used to couple a deterministic Boltzmann solver for the solution of the distribution function f sufficiently accurate for particular flows [24]. In this way we hope to simulate nonequilibrium flows with a wide range of the Knudsen number and the Mach number and with strong expansions, and this is the subject of our future investigation.

Acknowledgments

References

[1] Holden, M., "Experimental Studies of Laminar Separated Flows Induced by Shock Wave/Boundary Layer and Shock/Shock Interaction in Hypersonic Flows for CFD Validation," AIAA Paper 2000-0930, 2000.

[2] Bird, G. A., *Molecular Gas Dynamics and the Direct Simulations of Gas Flows*, Oxford Science, Oxford, U.K., 1994.

[3] Boyd, I., and Gokcen, T., "Evaluation of Thermochemical Models for Particle and Continuum Simulations of Hypersonic Flow," AIAA Paper 1992-2954, 1992.

[4] Bergemann, F., and Brenner, G., "Investigation of Wall Effects in Near Continuum Hypersonic Flow Using the DSMC Method," AIAA Paper 1994-2020, 1994.

[5] Ivanov, M. S., and Gimelshein, S. F., "Computational Hypersonic Rarefied Flows," *Annual Review of Fluid Mechanics*, Vol. 30, 1998, pp. 469–505.
doi:10.1146/annurev.fluid.30.1.469

[6] Wu, J.-S., and Tseng, K.-C., "Parallel Pariticle Simulation of the Near-Continuum Hypersonic Flows over Compression Ramps," *Journal of Fluids Engineering*, Vol. 125, No. 1, 2003, pp. 181–188.
doi:10.1115/1.1523068

[7] Xu, K., *Gas-Kinetic Schemes for Unsteady Compressible Flow Simulations*, Vol. 1998-03, The 29th Computational Fluid Dynamics, VKI Lecture Series, von Karman Institute for Fluid Dynamics, Rhode-St-Genèse, Belgium, 1998, pp. 1–202.

[8] Xu, K., "A Gas-Kinetic BGK Scheme for the Navier-Stokes Equations and Its Connection with Artificial Dissipation and Godunov Method," *Journal of Computational Physics*, Vol. 171, No. 1, 2001, pp. 289–335.
doi:10.1006/jcph.2001.6790

[9] Ohwada, T., and Xu, K., "The Kinetic Scheme for the Full-Burnett Equations," *Journal of Computational Physics*, Vol. 201, No. 1, 2004, pp. 315–332.
doi:10.1016/j.jcp.2004.05.017

[10] Xu, K., and Li, Z. H., "Microchannel Flow in the Slip Regime: Gas-Kinetic BGK-Burnett Solutions," *Journal of Fluid Mechanics*, Vol. 513, Aug. 2004, pp. 87–110.
doi:10.1017/S0022112004009826

[11] Gorchakova, N., Kuznetsov, L., Yarygin, V., Chanetz, B., Pot, T., Bur, R., Taran, J. P., Pignche, D., Schulte, D., and Moss, J., "Progress in Hypersonic Studies Using Electronic-Beam-Excited X-Ray Detection," *AIAA Journal*, Vol. 40, No. 4, 2002, pp. 593–598.

[12] Bird, G. A., "Aspects of the Structure of Strong Shock Waves," *Physics of Fluids*, Vol. 13, No. 5, 1970, pp. 1172–1177.
doi:10.1063/1.1693047

[13] Alsmeyer, H., "Density Profiles in Argon and Nitrogen Shock Waves Measured by the Absorption of an Electron Bean," *Journal of Fluid Mechanics*, Vol. 74, April 1976, pp. 497–513.
doi:10.1017/S0022112076001912

[14] Harris, S., *An Introduction to the Theory of the Boltzmann Equation*, Dover, Mineola, NY, 2004.

[15] Bhatnagar, P., Gross, E., and Krook, M., "A Model for Collision Processes in Gases," *Physical Review*, Vol. 94, No. 3, 1954, pp. 511–525.
doi:10.1103/PhysRev.94.511

[16] van Leer, B., "Towards the Ultimate Conservative Difference Scheme 2. Monotonicity and Conservation Combined in a Second Order Scheme," *Journal of Computational Physics*, Vol. 14, No. 4, 1974, pp. 361–370.
doi:10.1016/0021-9991(74)90019-9

[17] Xu, K., and Tang, L., "Nonequilibrium Bhatnagar-Gross-Krook Model for Nitrogen Shock Structure," *Physics of Fluids*, Vol. 16, No. 10, 2004, pp. 3824–3827.
doi:10.1063/1.1783372

[18] Xu, K., and Josyula, E., "Continuum Formulation for Non-Equilibrium Shock Structure Calculation," *Communications in Computational Physics*, Vol. 1, No. 3, 2006, pp. 425–450.

[19] Rosenau, P., "Extending Hydrodynamics via the Regularization of the Chapman-Enskog Expansion," *Physical Review A*, Vol. 40, No. 12, 1989, pp. 7193–7196.
doi:10.1103/PhysRevA.40.7193

[20] Elliot, J. P., "On the Validity of the Navier-Stokes Relation in a Shock Wave," *Canadian Journal of Physics*, Vol. 53, No. 6, 1975, pp. 583–586.

[21] Woods, L. C., *An Introduction to the Kinetic Theory of Gases and Magnetoplasmas*, Oxford University Press, Oxford, U.K., 1993.

[22] Li, Q. B., Fu, S., and Xu, K., "Application of Gas-Kinetic Scheme with Kinetic Boundary Conditions in Hypersonic Flow," *AIAA Journal*, Vol. 43, No. 10, 2005, pp. 2170–2176.

[23] Druguet, M.-C., Candler, G. V., and Nompelis, I., "Effects of Numerics on Navier-Stokes Computations of Hypersonic Double-Cone Flows," *AIAA Journal*, Vol. 43, No. 3, 2005, pp. 616–623.

[24] Kolobov, V. I., Arslanbekov, R. R., Aristov, V. V., Frolova, A. A., and Zabelok, S. A., "Unified Solver for Rarefied and Continuum Flows with Adaptive Mesh and Algorithm Refinement," *Journal of Computational Physics*, Vol. 223, No. 2, 2007, pp. 589–608.
doi:10.1016/j.jcp.2006.09.021

I. Boyd
Associate Editor